

Central Lancashire Online Knowledge (CLoK)

Title	THE COUNTERSTREAMING INSTABILITY IN DWARF ELLIPTICAL GALAXIES WITH OFF-CENTER NUCLEI1
Туре	Article
URL	https://clok.uclan.ac.uk/id/eprint/17007/
DOI	
Date	2004
Citation	De Rijcke, Sven and Debattista, Victor P (2004) THE COUNTERSTREAMING INSTABILITY IN DWARF ELLIPTICAL GALAXIES WITH OFF-CENTER NUCLEI1. Astrophysical Journal, 603. L25-L28. ISSN 0004-637X
Creators	De Rijcke, Sven and Debattista, Victor P

It is advisable to refer to the publisher's version if you intend to cite from the work.

For information about Research at UCLan please go to http://www.uclan.ac.uk/research/

All outputs in CLoK are protected by Intellectual Property Rights law, including Copyright law. Copyright, IPR and Moral Rights for the works on this site are retained by the individual authors and/or other copyright owners. Terms and conditions for use of this material are defined in the http://clok.uclan.ac.uk/policies/

THE COUNTERSTREAMING INSTABILITY IN DWARF ELLIPTICAL GALAXIES WITH OFF-CENTER NUCLEI¹

SVEN DE RIJCKE²

Sterrenkundig Observatorium, Universiteit Gent, Krijgslaan 281, S9, B-9000 Gent, Belgium; sven.derijcke@ugent.be

AND

VICTOR P. DEBATTISTA

Institut für Astronomie, ETH Hönggerberg, HPF G4.2, CH-8093 Zürich, Switzerland; debattis@phys.ethz.ch Received 2003 December 5; accepted 2004 January 21; published 2004 February 12

ABSTRACT

In many nucleated dwarf elliptical galaxies (dE,N's), the nucleus is offset by a significant fraction of the scale radius with respect to the center of the outer isophotes. Using a high-resolution N-body simulation, we demonstrate that the nucleus can be driven off-center by the m=1 counterstreaming instability, which is strong in flattened stellar systems with zero rotation. The model develops a nuclear offset on the order of 30% of the exponential scale length. We compare our numerical results with the photometry and kinematics of FCC 046, a Fornax Cluster dE,N with a nucleus offset by 1".2; we find good agreement between the model and FCC 046. We also discuss mechanisms that may cause counterrotation in dE,N's and conclude that the destruction of box orbits in an initially triaxial galaxy is the most promising.

Subject headings: galaxies: dwarf — galaxies: evolution — galaxies: individual (FCC 046) — galaxies: kinematics and dynamics — galaxies: nuclei — galaxies: structure

1. INTRODUCTION

Dwarf elliptical galaxies (dE's), faint, low surface brightness galaxies with smooth elliptical isophotes, are the most common type of galaxy in clusters and groups of galaxies (see Ferguson & Binggeli 1994). In hierarchical models of cosmological structure formation, dwarf galaxies form first and subsequently merge to form larger galaxies. Understanding their formation and evolution is therefore vital to a complete picture of structure formation. There is evidence that dE's constitute a heterogeneous class of objects, kinematically (rotating vs. unrotating; Geha, Guhathakurta, & van der Marel 2003), chemically (Michielsen et al. 2003), and morphologically (Barazza, Binggeli, & Jerjen 2002). About half of the dE's harbor a central bright nucleus and are called nucleated dE's (dE,N's); these appear to be significantly older than normal elliptical galaxies and nonnucleated dE's (Rakos & Schombert 2004). Upon tidal stripping, their nuclei have been suggested as sources of both the recently discovered ultracompact dwarfs (Phillipps et al. 2001) and massive globular clusters like ω Cen (Gnedin et al. 2002). In ~20% of Virgo dE,N's, the nucleus is significantly displaced with respect to the center of the outer isophotes, typically by ~1" (~100 pc; Binggeli, Barazza, & Jerjen 2000). There is a tendency for the displacement to increase with decreasing surface brightness, but no relation between nuclear displacement and any other structural or environmental parameter has been found.

Various models have been proposed to explain these offset nuclei. In this Letter, we investigate whether the lopsided (m=1) counterstreaming instability can reproduce a dE,N with an off-center nucleus. This instability has been known since Zang & Hohl (1978) and has been studied analytically (Sawamura 1988; Palmer & Papaloizou 1990) and with N-body simulations (Merritt & Stiavelli 1990; Levison, Duncan, & Smith 1990; Sellwood & Merritt 1994; Sellwood & Valluri

1997). Sellwood & Valluri (1997) do not detect it in systems rounder than E6, which is mainly the result of their rounder models being stabilized by a higher radial pressure. On the other hand, Merritt & Stiavelli (1990) find lopsidedness developing in systems as round as E1 but with negligible radial pressure. Partial rotation only introduces a pattern speed in an otherwise purely growing instability; simulations show that the lopsidedness produced by the instability is long-lived.

We use a realistic multicomponent *N*-body model to generate a lopsided system that we then compare with observations. In § 2 we present the *N*-body model, and in § 3 we compare it with the photometry and kinematics of FCC 046, an example of such a dE,N with an offset nucleus. In § 4 we discuss ways in which counterrotation may arise in dE,N's.

2. N-BODY SIMULATION

We have been using N-body simulations to explore the counterstreaming instability as a mechanism for producing lopsided dE,N's. We have performed both fully self-consistent simulations with live nucleus, disk, and halo run on a tree code and restricted simulations with rigid halos run on a grid code; both types of simulations will be presented elsewhere. Here we present only one simulation that happens to match FCC 046 best, consisting of live disk and nucleus components inside a rigid halo. The rigid halo was represented by a spherical logarithmic potential with core radius r_c and asymptotic circular velocity v_0 . The initial disk was modeled by an exponential disk of mass M_d , scale length R_d , Gaussian thickness z_d , and truncated at R_r . The nucleus of mass M_n was generated by iteratively integrating a distribution function in the global potential (Prendergast & Tomer 1970). We used a distribution function of the form $f(x, v) \propto \{[-E(x, v)]^{1/2} - (-E_{\text{max}})^{1/2}\}$. Here $E_{\text{max}} =$ $\Phi_{\rm tot}(r_{\rm u})$, the total potential at the nucleus truncation radius, $r_{\rm u}$, in the disk midplane. Initial disk kinematics were set up using the epicyclic approximation to give Toomre Q = 1.3. Vertical equilibrium was obtained by integrating the vertical Jeans equation. The disk and nucleus were represented by 36.8×10^5 and 3.2×10^5 equal-mass particles, respectively. After setup, we switched the direction of the velocity for half the particles,

¹ Based partly on observations collected at the European Southern Observatory, Paranal, Chile (ESO Large Program 165.N 0115).

² Research Postdoctoral Fellow of the Fund for Scientific Research, Flanders, Belgium (FWO).

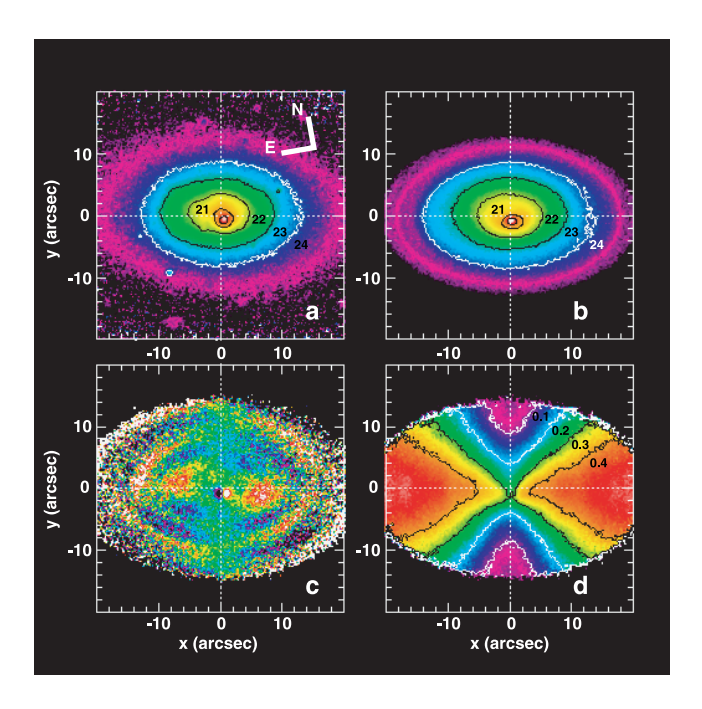


FIG. 1.—(a) *B*-band image of FCC 046; (b) surface brightness of the *N*-body model at t=150. The isophotes are spaced by 1 mag arcsec⁻², with the $\mu_B=24$ mag arcsec⁻² isophote drawn in white. Panels c and d show the model's velocity field and the velocity dispersion field, respectively. The velocity field perturbations have an m=2 symmetry and range between -0.06 (*black*) and +0.06 (*white*), corresponding to $\pm 0.1v_{circ}$.

producing an unrotating disk and a rotating nucleus. We used a quiet start (Sellwood 1983) to cancel spurious momenta and angular momenta.

In our units, where $R_d = M(= M_n + M_d) = G = 1$, which give a unit of time $(R_d^3/GM)^{1/2}$, we set $z_d = 0.2$, $R_t = 5$, $r_n = 0.78$, $r_c = 5$, and $v_0 = 0.648$. The simulation was run on a three-dimensional cylindrical polar grid code (described in Sellwood & Valluri 1997) with $N_R \times N_\phi \times N_z = 60 \times 64 \times 64$ 225. The vertical spacing of the grid planes was $\delta z =$ 0.0125. We used Fourier terms up to m = 8 in the potential, which was softened with the standard Plummer kernel, of softening length $\epsilon = 0.0125$. Time integration was performed with a leapfrog integrator using a fixed time step $\delta t = 0.006$. To scale units to FCC 046, we note that its surface brightness profile declines exponentially with scale length $R_d = 4''.1 \approx$ 0.4 kpc. We estimated the stellar mass of FCC 046 at $M \approx$ $1.0 \times 10^9 \ M_{\odot}$, given a *B*-band total luminosity $L_B = 2 \times 10^9 \ M_{\odot}$ $10^8~L_{B,\,\odot}$ and using a *B*-band mass-to-light ratio $M/L_B \approx 5$ $M_{\odot}/L_{B,\odot}$, typical for an old (15 Gyr), rather metal-poor ([Fe/ H] = -0.5) stellar population. With this scale length and mass, the unit of time corresponds to $(R_d^3/GM)^{1/2} \approx 4$ Myr, and the velocity unit becomes $(GM/R_d)^{1/2} \approx 100$ km s⁻¹.

The global lopsidedness of the model, as measured by the amplitude of the m=1 term in a Fourier expansion of the surface density, rose exponentially with time, saturating at $t \approx 70$, for an e-folding time $\tau=5.67$. The angular momentum of the disk and the orbital angular momentum of the nucleus increase at the expense of the nucleus's internal (rotational) angular momentum. By the end of the simulation, the nucleus has lost approximately 20% of its initial internal angular momentum. However, the resulting orbital velocity of the nucleus $(v_{\text{nuc}} \approx 0.01)$ is only a few percent of the local circular velocity $(v_{\text{circ}} \approx 0.35)$, so that dynamical friction against a live dark

matter halo is not likely to damp the instability, as is also borne out by the live halo simulations.

3. FCC 046: A CASE STUDY

FCC 046 is an $m_B = 15.99$ dE4,N in the Fornax Cluster. Photometry and long-slit spectra, with an instrumental broadening $\sigma_{\rm instr} = 30$ km s⁻¹, in the wavelength region containing the strong absorption lines of the near-infrared Ca II triplet, were observed at the Very Large Telescope with FORS2 in November of 2001 (photometry) and 2002 (spectroscopy). Seeing conditions were typically 0″.8 FWHM. A detailed analysis of the photometry has been presented in De Rijcke et al. (2003b), while details of the kinematics of FCC 046 will be presented elsewhere. Additionally, the *Hubble Space Telescope* (HST) archives contain WFPC2 images of FCC 046 in the filters F814W and F555W. Availability of all these data was the sole reason for selecting this object.

FCC 046 contains a bright nucleus, which is displaced by 1".2 with respect to the outer isophotes, or 30% of R_d . The lopsidedness involves not just the nucleus but extends to $\sim 2R_d$. Color maps show no traces of large amounts of dust but suggest the presence of a blue stellar population. The H α image reveals ionized emission regions, evidence of ongoing star formation, within $\sim 1R_d$. The position of the blue stellar population does not coincide with the lopsidedness of FCC 046 and is not likely to be the cause of it (although it may be a consequence of it). FCC 046 is in the outskirts of the Fornax Cluster; its nearest neighbors are dwarfs over 100 kpc (in projection) away, and the nearest large galaxy is more than 200 kpc distant. Interactions are therefore not likely to account for its morphology, unless a weakly damped mode has been excited (Weinberg 1994). The kinematics of FCC 046 (mean velocity and velocity dispersion) were extracted from the spectra following the method discussed in De Rijcke et al. (2003a). Despite its E4 flattening, the main body of FCC 046 has zero mean rotation. The lack of rotation excludes the possibility that the eccentric instability (Adams, Ruden, & Shu 1989; Miller & Smith 1992; Taga & Iye 1998) is responsible for the lopsidedness.

The nucleus is resolved by HST; it has a FWHM = 0".27, significantly larger than the FWHM = 0.15 of the stars in the same image, and therefore cannot be a foreground star. The nucleus has the same systemic velocity as the galaxy, which rules out a chance projection of a background object. It comprises ~10% of the B-band luminosity of FCC 046 and is therefore probably quite massive. We can use the fact that the outer isophotes of the N-body model do not move appreciably, and that their center coincides with the model's center of mass (COM), to estimate the relative mass-to-light (M/L) ratios of the disk and nucleus. In order for the mean position of the Bband light distribution to coincide with the COM, the M/L ratio of the nucleus has to be less than half that of the disk. If the disk consists of an old, metal-poor population with $M/L_B \approx 5$ $M_{\odot}/L_{B,\odot}$, this would mean that the nucleus has $M/L_B < 2$ $M_{\odot}/L_{B,\odot}$, typical for a very young stellar population (age < 2–3 Gyr). This is consistent with the blue color of the nucleus and its strong Pa absorption (Michielsen et al. 2003). The rotation axis of the nucleus is not aligned with that of the galaxy's main body, showing evidence of minor-axis rotation with an amplitude of ≈ 5 km s⁻¹.

The surface density, the velocity field, and the velocity dispersion field of the N-body model at t = 150 are presented in Figure 1. The viewing angle and the spatial scale were chosen

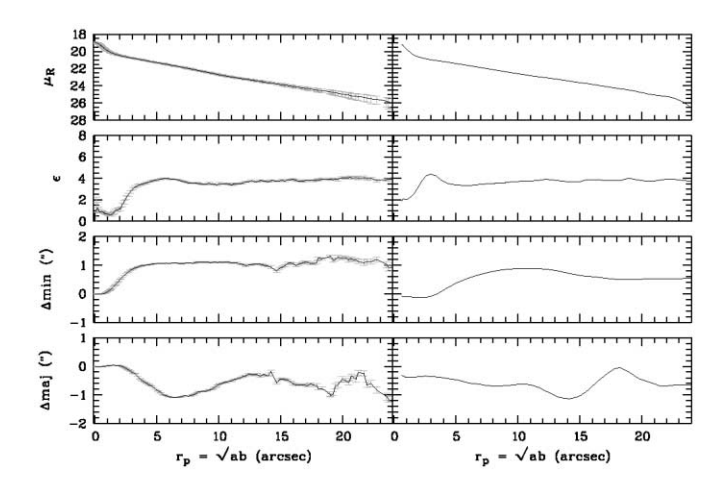


Fig. 2.—Surface photometry of FCC 046 (*left panels*), compared with the *N*-body model (*right panels*); a and b are, respectively, the semimajor and minor axes of the isophotes. In the top panels, the *R*-band surface brightness (in units of mag arcsec⁻²) of FCC 046 is compared with that of the model. In the next set of panels, the ellipticity $\epsilon = 10(1 - b/a)$ of the isophotes is shown. In the bottom panels, the position of the center of the isophotes is presented; Δ maj and Δ min (in arcseconds) quantify the position of the isophotes along the major and minor axes, centered on the nucleus.

such that the model's surface density gives a fair approximation of the *B*-band image of FCC 046. The nucleus is offset by $\sim 1''$ to the southwest with respect to the outer isophotes, and, in response, there is an excess in the disk density to the northeast, as in FCC 046. Clearly, the instability engenders a global response of the whole stellar system. In Figure 2, we compare the surface photometry of FCC 046 with the N-body model (convolved with a Gaussian to mimic the seeing conditions of the observations) in greater detail. Simply shifting the magnitude zero point of the N-body model and applying the same spatial scale as in Figure 1 sufficed to match the surface brightness profile of FCC 046. As in FCC 046, the isophote centers of the model oscillate along the major axis; in the model, this keeps the total COM fixed. Just outside the nucleus, the density contours have a distorted shape that, in projection, results in the isophotes being flatter (around ~5" in FCC 046 and around \sim 3" in the model) than at larger radii. On the whole, the model successfully reproduces gross features in the surface photometry of FCC 046.

Figure 1 shows that while the model's mean velocity is zero, bisymmetric perturbations of order ~0.06 are present. The velocity dispersion profile is asymmetric, rising less rapidly toward the left side of the model, in the direction of the excess light. The apparent flattening of FCC 046 and its zero mean rotation already hint at two equal-mass counterstreaming stellar populations. Although at the limit of what can be done, given the spectral resolution and the low signal-to-noise ratio (S/N) of the data, the strongest Ca II absorption line in the majoraxis spectrum appears split into two distinct lines (see Fig. 3), separated by 70 ± 25 km s⁻¹; the other, weaker lines have much lower S/Ns. This absorption line is unaffected by the bright sky OH emission lines. (If a badly removed sky line were the cause of the line splitting, it would also manifest itself in the center of the galaxy and in the minor-axis spectrum, which is not the case.) What is particularly compelling about these data is that the apparent bimodality is present (and absent) where the model predicts it should be (before the signal disappears in the noise) and that we see similar splitting in three different spatial bins. To illustrate this, in Figure 3 we plot the

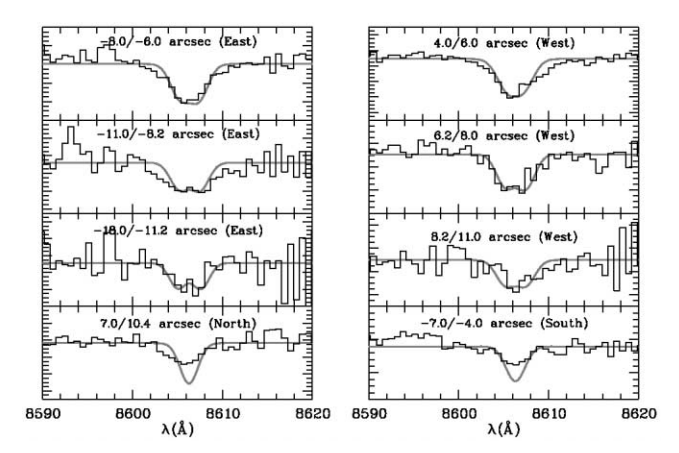


FIG. 3.—Part of the spectrum of FCC 046, around the strongest Ca II absorption line. The radial bins over which the spectrum has been summed to boost the S/N are indicated in the figure (left top three panels: along the major axis, toward the east; right top three panels: along the major axis, toward the west; bottom panels: along minor axis, toward the north (left) and toward the south (right). Radii are measured from the nucleus. Observed spectrum: black line; model spectrum: gray line (see text for details). This absorption line appears split into two distinct lines, separated by $70 \pm 25 \text{ km s}^{-1}$, in the outermost major axis spectra. The S/N in these panels varies from 5–10 to 20–25; adjacent spectra from the left and right panels have comparable S/Ns. The minor-axis spectra have the same continuum level as the outermost majoraxis spectra. Clearly, the Ca II line does not appear split in the minor-axis spectra. The model reproduces rather well the major-axis line width and the observed line splitting.

observed spectrum and the model spectrum, consisting of a flat continuum and a very narrow (δ -function) absorption line, broadened with the FORS2 instrumental profile and the model's line-of-sight velocity distribution (LOSVD), summed over the same spatial bins as the observed spectrum. We did not use an observed stellar template since the width of the individual LOSVD peaks is smaller than 1 FORS2 pixel, making an accurate calculation of a synthetic galaxy spectrum impossible. Except for underestimating the minor-axis velocity dispersion, the model reproduces rather well the major-axis line widths and the observed line splitting.

However, these observations, while very suggestive, need to be corroborated at higher spectral resolution to resolve the two peaks in the LOSVDs. In Figure 4, we present a mosaic of LOSVDs at different points in the model. Moving out along the major axis, the LOSVDs become more double-peaked because of the increasing velocity separation between the two counterstreaming stellar populations and the declining velocity dispersion. The small velocity-field perturbations of Figure 1 are reflected here in the LOSVDs being slightly asymmetric. Although the details of the LOSVD field in Figure 4 are model-dependent, an observational confirmation of its salient features would lend considerable support to the hypothesis that the counterstreaming instability is responsible for off-center nuclei in dE,N's.

4. DISCUSSION

If the counterstreaming instability is indeed working in a sizable fraction of the dE,N's to drive nuclei off-center, it is natural to ask why these dE's have counterrotation in the first place. The first detections of counterrotation in galaxy disks (Rubin, Graham, & Kenney 1992; Merrifield & Kuijken 1994) lead to the hypothesis that the capture of gas with retrograde rotation and subsequent star formation produced two counterrotating stellar disks. This hypothesis predicts stellar popula-

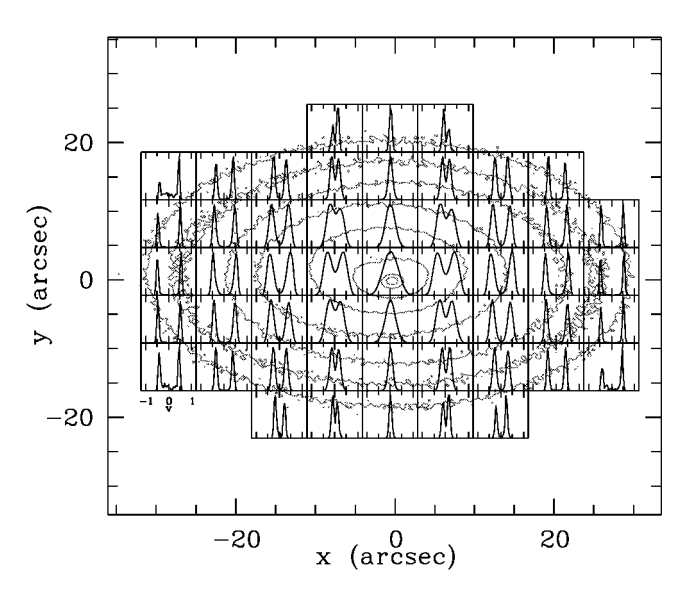


Fig. 4.—Mosaic of the LOSVDs at different points in the projected model (the middle panel is centered on the center of the outer isophotes). The big and small tick marks indicate a velocity $v=\pm 1$ and $v=\pm 0.5$, respectively, as indicated below the leftmost panel. The isophotes of the model, separated by 1 mag arcsec⁻², are plotted in gray scale.

tions of different ages and metallicities. Generally, the two disks will not have identical masses, so some net rotation is expected; this is, therefore, an unlikely explanation for FCC 046.

Tremaine & Yu (2000) suggested that counterrotation is produced when a triaxial halo with an initially retrograde pattern speed slowly changes to a prograde pattern speed. However, this situation probably does not occur very often. Moreover, this mechanism requires evolution on long timescales of $\sim 10^{10}$ yr and hence requires dE,N's to be old and unperturbed.

A more likely mechanism is the destruction of box orbits, which are the backbone of any slowly rotating triaxial mass distribution, by a growing nucleus. Stars on box orbits come very close to the nucleus and thus can be scattered into loop orbits; conservation of angular momentum then requires that direct and retrograde loop orbits be equally populated (Evans & Collett 1994; Merritt & Quinlan 1998). If the nucleus has a mass larger than 2% of the total mass of the galaxy, evolution toward an axisymmetric shape requires a few crossing times $(\approx 10^7 - 10^8 \text{ yr})$, while our simulations show that the counterstreaming instability develops on similar timescales. Late infall of gas (Conselice et al. 2003), perhaps as a result of harassment (Moore et al. 1996; Mayer et al. 2001) or globular clusters (Lotz et al. 2001), may be responsible for growing the nucleus. If this explanation holds, then the two counterrotating stellar populations should have equal scale lengths and chemical properties and nearly equal mass. Additionally, the nucleus may retain some of its initial angular momentum; we note that the nucleus of FCC 046 is indeed rotating.

To summarize, using *N*-body simulations, we have shown that the counterstreaming instability is a viable explanation for at least the dE,N galaxy FCC 046. The models can produce offsets as large as observed and can successfully reproduce distinctive features in the surface photometry of FCC 046, such as the oscillation of isophote centers. Although at the limit of what can reliably be extracted from the spectra, we find a tantalizing hint of counterstreaming in the major-axis spectrum of this galaxy, which, however, needs to be corroborated at higher spectral resolution.

V. P. D. thanks the Sterrenkundig Observatorium for their hospitality during an early stage of this project. We thank Stelios Kazantzidis and Anna Pasquali for useful discussions and the referee, O. Gnedin, for the suggested improvements.

REFERENCES

Adams, F. C., Ruden, S. P., & Shu, F. H. 1989, ApJ, 347, 959 Barazza, F. D., Binggeli, B., & Jerjen, H. 2002, A&A, 391, 823 Binggeli, B., Barazza, F., & Jerjen, H. 2000, A&A, 359, 447 Conselice, C. J., O'Neil, K., Gallagher, J. S., & Wyse, R. G. 2003, ApJ, 591, De Rijcke, S., Dejonghe, H., Zeilinger, W. W., & Hau, G. K. T. 2003a, A&A, 400, 119 De Rijcke, S., Zeilinger, W. W., Dejonghe, H., & Hau, G. K. T. 2003b, MNRAS, 339, 225 Evans, N. W., & Collett, J. L. 1994, ApJ, 420, L67 Ferguson, H. C., & Binggeli, B. 1994, A&A Rev., 6, 67 Geha, M., Guhathakurta, P., & van der Marel, R. P. 2003, AJ, 126, 1794 Gnedin, O. Y., Zhao, H.-S., Pringle, J. E., Fall, S. M., Livio, M., & Meylan, G. 2002, ApJ, 568, L23 Levison, H. F., Duncan, M. J., & Smith, B. F. 1990, ApJ, 363, 66 Lotz, J. M., Telford, R., Ferguson, H. C., Miller, B. W., Stiavelli, M., & Mack, J. 2001, ApJ, 552, 572 Mayer, L., Governato, F., Colpi, M., Moore, B., Quinn, T., Wadsley, J., Stadel, J., & Lake, G. 2001, ApJ, 559, 754

Merrifield, M. R., & Kuijken, K. 1994, ApJ, 432, 575

Merritt, D., & Quinlan, G. D. 1998, ApJ, 498, 625 Merritt, D., & Stiavelli, M. 1990, ApJ, 358, 399 Michielsen, D., De Rijcke, S., Dejonghe, H., Zeilinger, W. W., & Hau, G. K. T. 2003, ApJ, 597, L21 Miller, R. H., & Smith, B. F. 1992, ApJ, 393, 508 Moore, B., Katz, N., Lake, G., Dressler, A., & Oemler, A., Jr. 1996, Nature, 379, 613 Palmer, P. L., & Papaloizou, J. 1990, MNRAS, 243, 263 Phillipps, S., Drinkwater, M., Gregg, M., & Jones, J. 2001, ApJ, 560, 201 Prendergast, K. H., & Tomer, E. 1970, AJ, 75, 674 Rakos, K., & Schombert, J. 2004, AJ, in press (astro-ph/0312075) Rubin, V. C., Graham, J. A., & Kenney, J. D. P 1992, ApJ, 394, L9 Sawamura, M. 1988, PASJ, 40, 279 Sellwood, J. A. 1983, J. Comput. Phys., 50, 337 Sellwood, J. A., & Merritt, D. 1994, ApJ, 425, 530 Sellwood, J. A., & Valluri, M. 1997, MNRAS, 287, 124 Taga, M., & Iye, M. 1998, MNRAS, 299, 111 Tremaine, S., & Yu, Q. 2000, MNRAS, 319, 1 Weinberg, M. D. 1994, ApJ, 421, 481 Zang, T. A., & Hohl, F. 1978, ApJ, 226, 521